Sustainable Chemistry and Pharmacy 39 (2024) 101599

Contents lists available at ScienceDirect

Sustainable Chemistry and Pharmacy

journal homepage: www.elsevier.com/locate/scp

Salt slag and rice husk ash as raw materials in zeolite synthesis: Process optimization using central composite rotational design

Magali Teresinha Ritter[a, b], María Ángeles Lobo-Recio[b, c], Isabel Padilla[a, *], Maximina Romero[a], Aurora López-Delgado[a]

[a] Department of Materials, Eduardo Torroja Institute for Construction Sciences (IETcc-CSIC), Serrano Galvache Street, 4, 28033, Madrid, Spain
[b] Department of Sanitary and Environmental Engineering, Federal University of Santa Catarina (UFSC), Campus Reitor João David Ferreira Lima, 88040-900, Florianópolis, SC, Brazil
[c] Department of Energy and Sustainability, Federal University of Santa Catarina (UFSC), Campus Araranguá, Rod. Gov. Jorge Lacerda, 3201, Jardim das Avenidas, 88.906-072, Araranguá, SC, Brazil

ARTICLE INFO

Handling Editor: Fabio Aricò

Keywords:
Waste-based zeolites
NaP zeolite
Hazardous waste
Salt slag
Rice husk ash
Central composite rotational design

ABSTRACT

The growing demand of zeolites for many industrial applications has led to a search for eco-friendly alternatives for their production, in an attempt to reduce costs, save natural resources and alleviate the associated environmental impacts. In the present study, hazardous aluminum salt slag (aluminum source) and rice husk ash (silicon source) were used as secondary raw materials to synthesize sustainable NaP-type zeolites through a hydrothermal process. A central composite rotational experimental design was applied to evaluate the effect of the reaction time and hydrothermal temperature on the obtained zeolites crystallinity. Using the proposed experimental design, temperatures between 85 and 115 °C and different reaction times (2–28 h) were tested. It was found that the interaction between the variables (time and temperature) and both variables, independently, exerted a significant influence on the crystallinity of the zeolites. The optimal experimental conditions (105 °C and 20 h), statistically determined, enabled a high degree of crystallinity (>73%) to be achieved. Thus, the use of hazardous aluminum and agri-food wastes as unconventional precursors for the production of zeolites represents a sustainable alternative to manage these wastes, by transforming them into secondary raw materials.

1. Introduction

Zeolites are crystalline materials with a three-dimensional structure composed of AlO_4 and SiO_4 tetrahedra. Due to their unique properties, they have been extensively used in many industrial applications as adsorbents, catalysts, membrane materials, ion exchangers, and chemical sensors, among others (Abdel-Hameed et al., 2020). Zeolites represent the most important group of microporous materials (Xu et al., 2007), and their global demand is increasing, especially stimulated by the detergent industry, where synthetic zeolites are employed as an alternative to replace contaminating phosphate agents, following more restrictive regulations implemented in several countries (Markets and Markets, 2023). Zeolites can be obtained from natural deposits or synthesized from a wide variety of aluminum and silicon sources (Xu et al., 2007). According to a recent report by Markets and Markets, (2023), the global zeolite market was 4872 metric tons (12.1 billion dollars) in 2021 and an estimated 5453 metric tons (14.1 billion dollars) in 2026, of which 5.9 billion dollars correspond to synthetic zeolites.

* Corresponding author. Department of Materials, Eduardo Torroja Institute for Construction Sciences, IETcc-CSIC, Serrano Galvache Street, 4, 28033, Madrid, Spain.
E-mail address: isabel.padilla@ietcc.csic.es (I. Padilla).

https://doi.org/10.1016/j.scp.2024.101599
Received 27 February 2024; Received in revised form 18 April 2024; Accepted 28 April 2024
Available online 8 May 2024

Concerning synthetic zeolites, research efforts have recently focused on the production of zeolites using different wastes as unconventional raw materials. Converting waste into functional value-added products is of great importance for sustainability and environmental protection (Shu et al., 2023). A variety of wastes have been used in the zeolite synthesis, including coal fly ash, waste glass, alum sludge, rice husk, bauxite residue, etc. (Collins et al., 2020).

Among aluminum waste, salt slag is the main solid waste, generated in large quantities by the secondary aluminum industry (~0.5 tons of salt slag per ton of recycled aluminum produced) (Padilla et al., 2022). By 2027, it is estimated that more than 26 million metric tons of salt slag recycled aluminum will be generated worldwide (Statista, 2023), representing approximately 13 million metric tons of slat slag. The management of this waste is considered a major problem. The European Catalogue of Hazardous Waste (2001) classifies salt slag as a toxic and hazardous waste (code 10 03 08), and considered highly irritant, harmful, leachable and flammable (EWC, 2001). Salt slag contains a significant amount of harmful leachable salts and its disposal has negative effects on both the environment and human health, polluting soil and groundwater (Srivastava and Meshram, 2023). In addition, it is highly reactive in contact with water or even moisture in the air, leading to the formation of toxic gases, such as CH_4, NH_3, H_2, H_2S and PH_3, whose emissions into the atmosphere cause serious environmental damage (Tsakiridis, 2012). However, its aluminum-rich composition makes salt slag a potential candidate for zeolite synthesis. In this sense, in a preliminary study (Padilla et al., 2022), a NaP-type zeolite was synthesized using salt slag and a commercial sodium silicate as silicon source. The synthesis process was performed at 100 °C for 24 h. The as-obtained zeolite exhibited a specific surface area of 17 $m^2\ g^{-1}$, a cation exchange capacity (CEC) of 2.12 meq g^{-1} and a predominant pore size of 3.8 nm.

Regarding to silicon waste, rice husk ash (RHA) is a silicon-rich material and is considered one of the most abundant agri-food wastes. It results from the thermal transformation of rice husks, a readily available and inexpensive material. The Organization of the United Nations for Food and Agriculture (FAO, 2022) estimated that more than 31 million tons of rice husk ash would be generated in the world by the end of 2023. Although RHA is not considered a hazardous waste, its landfill disposal and slow biodegradation cause several environmental impacts. Thus, zeolite synthesis from RHA opens a new route for the use of this waste, which is presented as an alternative and low-cost substitute for commercial silica (Mallapur and Oubagaranadin, 2017; Mohamed et al., 2015; Tan et al., 2011; Tran-Nguyen et al., 2021; Vasconcelos et al., 2023). In this way, Mohamed et al. (2015) reported the synthesis of NaY zeolite, using RHA and commercial aluminate. The process involved extracting silica from the RHA through acid washing and alkali activation (NaOH) followed by a two-step synthesis in which a feedstock solution and a seed gel were prepared, kept at room temperature for 24 h and then mixed and stirred at 110 °C for the same period of time. In a similar way to the aforementioned authors, Tan et al. (2011) obtained NaY and NaA zeolites using RHA and commercial aluminate. The process consisted of preparing the seed and feedstock solution by adding the required amounts of reactants, stirring vigorously until completely mixed and then aging at room temperature for 24 h. The mixture of both solutions forms a gel that was kept at room temperature for 24 h and finally, using a Teflon bottle, heated to 100 °C for a further 5 h. The difference in the zeolitic material obtained was related to the silica extraction process; alkaline activation using NaOH pellets led to the formation of NaY-type zeolite, while with NaOH (1 M) solution, NaA zeolite was formed. Tran-Nguyen et al. (2021) obtained a NaX zeolite using RHA and commercial aluminum powder. The silicate solution was prepared by treating RHA with a 5 M NaOH solution at 90 °C for 3 h, and the aluminate solution was also produced by alkaline dissolution of the aluminum powder. The synthesis was carried out by mixing the two solutions under vigorous stirring (at 50 °C for 2 h) and heating the obtained gel at 90 °C for 4 h.

With regard to the methodologies used in zeolite synthesis, most studies report the use of processes involving several steps, as mentioned above. Furthermore, in most cases, zeolitic materials are synthesized from a single waste as a source of silicon or aluminum, supplementing the necessary content of the other precursor with chemical reagents. In this work, both hazardous salt slag and rice husk ash have been used as exclusive aluminum and silicon sources, respectively, and the hydrothermal synthesis of waste-based zeolites, more specifically NaP zeolite, was carried out in a single-step under mild conditions. To our knowledge, the combination of these two wastes has not been reported in the literature. Indeed, the process developed can be considered as a co-recycling of two different wastes. In order to determine the effect of the main synthesis parameters (time and temperature) on the crystallization of zeolites, a central composite rotational design (CCRD) was applied (Alaba et al., 2017). The use of experimental design is underexploited by researchers but represents an important optimization strategy for determining the optimal synthesis parameters, allowing the simultaneous analysis of factors at different levels and reducing the number of required experiments. Optimizing the experimental conditions is a crucial point in the synthesis of crystalline zeolites. The convencional orthogonal method, although extensively employed for optimizing operational parameters in Various processes, is not capable of generating a clear functional relationship between factors and response values, posing challenges in identifying the ideal parameter combination (Yi et al., 2010). In the present investigation, the CCRD was used to determine the optimal synthesis conditions and overcome these disadvantages of the traditional orthogonal method. The use of hazardous aluminum and agri-food wastes as less-common precursors for the production of zeolites is presented as a sustainable alternative to the waste management, generating value-added materials with promising applications, and greatly contributing to environmental preservation, circular economy, and industrial symbiosis.

2. Materials and methods

2.1. Characterization techniques

A wavelength dispersive X-ray fluorescence (XRF) spectrometer (Bruker, S8 Tiger) was used to determine the chemical composition of the raw materials. The composition of the silicate solution extracted from the RHA was analyzed by an inductively coupled plasma optical emission spectrometer (ICP-OES) (Spectro Arcos). Mineralogical characterization of the wastes and obtained zeolites

was performed by X-ray diffraction (XRD) using a Bruker D8 Advance Diffractometer with CuKα radiation, with 2θ from 5° to 60°, at a scan rate 2θ of 0.02°, 5 s per step. The crystallite sizes were calculated using the Scherrer equation (**Equation (1)**) (Scherrer, 1918):

$$D_{hkl} = {}^{K.\lambda}/_{FWHM.cos\ \theta} \quad (1)$$

where K is the constant of Scherrer (0.9), λ is the x-ray wavelength (0.154 nm), FWHM is the Full Width at Half Maximum (in rad) and θ corresponds to the diffraction angle (in rad) of the most intense reflection centered around 28.1° (2θ), corresponding to the hkl [301]. The FWHM was determined by non-linear fit to the Gauss function, using OriginPro 8.5 software. The degree of crystallinity and semiquantification of the crystalline phases of the zeolites was performed using Diffrac.Suite EVA software. The thermal behavior of rice husk ash was studied using thermogravimetric analysis and differential thermal analysis (TG/DTA) on a Thermoanalyzer model SDT-Q600 (TA Instruments), with a heating rate of 10 °C min^{-1} under an air flow of 100 mL min^{-1}. The morphology of the zeolites was examined by Scanning Electron Microscopy (SEM), using a Hitachi S4800 microscope equipped with an energy dispersive X-ray spectroscopy detector (EDS). The textural characterization of the zeolite was performed by determination of nitrogen adsorption/desorption isotherms at −196 °C in an ASAP 2010 Micromeritics system. The sample was previously outgassed at 250 °C in vacuum for 24 h. The specific surface area (S_{BET}) and pore size distribution was determined through multi-point measurements using the Brunauer-Emmett-Teller (BET) method and the Barrett-Joyner-Halenda (BJH) method, respectively. The external area (S_{Ext}) was calculated by the t-plot method from the slope of the linear fit in the thickness range (t) of 0.35–0.5 nm according to the Harkins-Jura equation. The NH_4^+ ion exchange method using a 1 M NH_4Cl solution (pH ~ 7) was applied to determine the cation exchange capacity (CEC) of the zeolites, with tests conducted in duplicate (NC 626, 2008).

2.2. Raw materials

Aluminum salt slag (ASS) and rice husk ash (RHA) were used as aluminum and silicon source, respectively, for the synthesis of zeolite type P ($Na_6Al_6Si_{10}O_{32}{\cdot}12H_2O$).

The as-received ASS (Alusigma S.A, Gijón, Spain) consisted of a dark-grayish granular solid (Fig. 1a), with a particle size distribution ranging from very fine powder (< 0.5 mm) to granules larger than 5.7 mm, and the major fraction (53%) composed of coarse grain sizes (1–4 mm). Due to its granulometric and compositional heterogeneity, salt slag was subjected to a grinding process in order to standardize the particle size (< 0.25 mm) and enable a better reaction in the synthesis stage. A sample of around 3 kg of ASS was divided into eight representative aliquots using a Laborette 27 Rotary Cone Sample Divider, with one of these aliquots used in the experiments. This procedure aimed to guarantee the reproducibility and accuracy of the results.

Due to its high NaCl content, ASS was subjected to a hydrolysis process (see Section **2.3**) before being used as a raw material in the synthesis of zeolites.

The as-received rice husk ash (RHA) (Herba Ricemills, Seville, Spain) consisted of a homogeneous dark powdery solid with some white fibers and a predominant particle size of 0.1–0.5 mm (Fig. 1c).

2.3. Pretreatment of waste materials

The salt slag was hydrolyzed in order to eliminate *(i)* excess salt that could interfere with the process of transforming the slag into zeolites and *(ii)* cause the reaction of the aluminum compounds, transforming them into oxides and thus releasing the corresponding gases (such as ammonia, hydrogen and hydrogen sulfide).

The hydrolysis of the aluminum salt slag was carried out by placing 300 g of sample in a volumetric flask and dripping distilled water using a peristaltic pump. After adding the corresponding volume of water, the suspension was maintained at a temperature of 90 °C under continuous stirring for 2 h. After filtering under pressure, the cake (hydrolyzed slag, HS) was dried for 24 h at 100 °C. HS (Fig. 1b) was the only source of aluminum used in the zeolite synthesis.

A silicate solution was prepared from calcined rice husk ash (Fig. 1d) in order to provide the silicon required for formation of zeolite. The extraction of silicon from CRHA was carried out by mixing 48 g of RHA with a 3 M NaOH solution in a Teflon-lined autoclave reactor (Parr, 1 L volume) and kept under constant stirring for a reaction time of 3 h at 120 °C. After the reaction, the products were filtered to separate the sodium silicate solution. The composition of the silicate solution was analyzed by inductively coupled plasma optical emission spectrometer (ICP-OES).

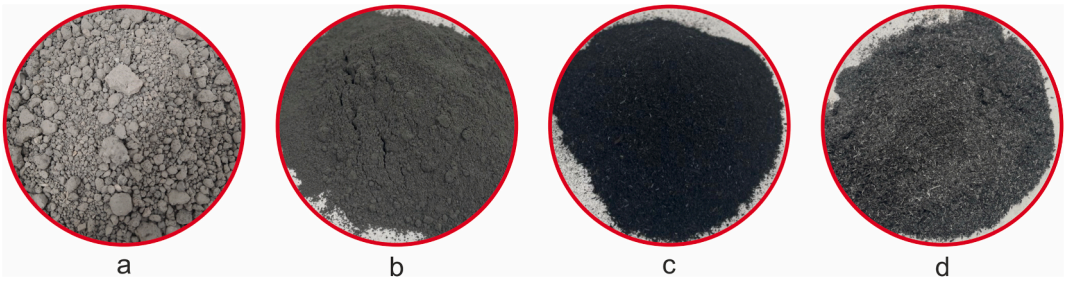

Fig. 1. Macroscopic appearance of the (a) aluminum salt slag (ASS), (b) hydrolyzed slag (HS), (c) rice husk ash (RHA) and (d) calcined rice husk ash (CRHA).

2.4. Synthesis of zeolites

The waste-based zeolites were produced following the procedure shown in Fig. 2. Synthesis was carried out in the $Na_2O–Al_2O_3–SiO_2–H_2O$ system by the conventional hydrothermal method. The reactants, solid aluminum hydrolyzed slag, and the silicate solution extracted from the CRHA, were mixed in appropriate proportions to provide the stoichiometric Si/Al ratio fot NaP-type zeolite ($Na_6Al_6Si_{10}O_{32}{\cdot}12H_2O$), and they were placed, along with the corresponding volumes of 1 M NaOH solution and distilled water, in the autoclave reactor. For the objective of synthesizing NaP type-zeolite, all the experiments were performed with continuous stirring and under autogenous pressure. Different temperatures (85–115 °C) and reaction times (2–28 h) were tested according to the experimental design (Table 1) presented in Section **2.5**. After the synthesis, the solid products were separated by filtration, rinsed with distilled water, and subjected to driying at 100 °C for 24 h.

2.5. Experimental design

Design of experiments is an important tool for modeling, developing, improving, and optimizing processes, determining the effects of factors on a response at different levels. Furthermore, this method minimizes the number of required experiments and allows the determination of the optimal factors values influencing the process (Kafshgari et al., 2017). In order to determine the optimal conditions for the hydrothermal synthesis of the zeolite, a central composite rotational design (CCRD) with two factors and two levels (2^2) was developed. Hydrothermal temperature and reaction time were considered as the independent variables influencing zeolite synthesis, and the degree of crystallinity of the obtained zeolites was chosen as the response (dependent variable). The CCRD was developed using the STATISTICA® 13.3 software. Eleven tests were carried out, using the factor scores (−1 and +1), which indicate the minimum and maximum level of each variable; 3 central points (0) and the axial portions (−1.414 and + 1.414), calculated by **Equation (2)**.

$$\alpha = (2^n)^{1/4} \tag{2}$$

where α is the axial distance from the central point and n is the number of independent variables ($n = 2$). Factor values at the central point (100 °C and 15 h) were determined based on preliminary tests. The variable levels used in this study are shown in Table 1. The statistical analysis of the experimental results were analyzed using the p-value, where values of 0.05 being statistically significant at the 95% confidence level. The optimal experimental conditions were determined based on the median of the statistical critical points.

3. Results and discussion

3.1. Characterization of raw and processed materials

The chemical composition of salt slag mainly consists of about 35 wt.% aluminum (expressed as Al_2O_3) and 18 wt.% Na_2O, along with chloride, according to the X-ray fluorescence (XRF) analysis presented in Table 2. The X-ray diffraction (XRD) pattern of the aluminum slag (Fig. 3), consistent with its chemical composition, shows the aluminum content distributed in different phases: corundum (Al_2O_3), aluminum nitride (AlN), metallic aluminum (Al) and spinel (Al_2MgO_4); and quartz (SiO_2). Salt slag exhibits pronounced

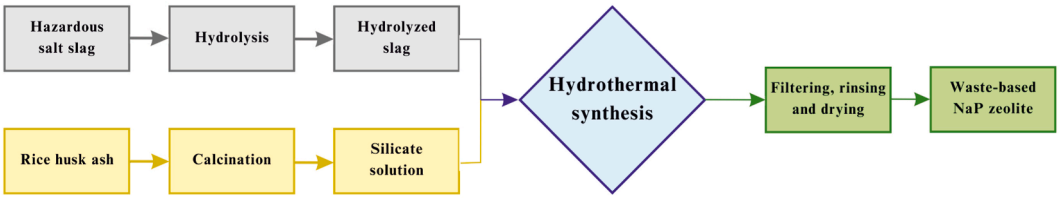

Fig. 2. Schematic procedure for the synthesis of waste-based zeolite.

Table 1
Levels of variables used for CCRD.

Variable	(-1.414)	(-1)	(0)	(+1)	(+1.414)
Hydrothermal temperature (°C)	85	90	100	110	115
Reaction time (h)	2	6	15	24	28

Table 2
Chemical composition (XRF, expressed as wt.% oxide) and loss of ignition (LOI) (%) of the aluminum salt slag (ASS), hydrolyzed slag (HS), as-received rice husk ash (RHA) and calcined rice husk ash (CRHA).

	Al_2O_3	SiO_2	Na_2O	Cl	MgO	CaO	Fe_2O_3	K_2O	ZnO	P_2O_5	TiO_2	CuO	LOI
ASS	35.5	6.4	18.3	16.7	5.1	3.9	1.7	0.5	0.4	<0.1	0.4	0.4	9.8
HS	63.5	7.7	1.6	1.5	7.9	4.5	3.0	0.2	0.8	<0.1	0.7	0.8	6.2
RHA	0.2	73.5	0.4	0.7	1.1	1.3	0.8	3.9	<0.1	1.4	–	<0.1	15.7
CRHA	0.3	89.7	0.4	<0.1	0.8	1.3	0.2	3.6	<0.1	1.7	–	–	0.2

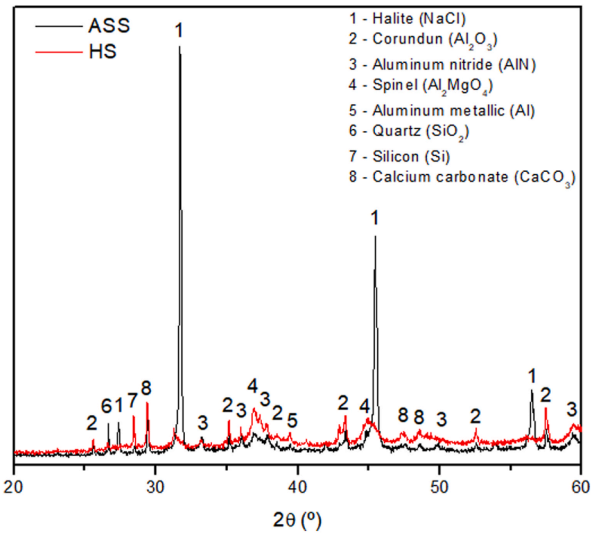

Fig. 3. XRD pattern of the aluminium salt slag (ASS) and hydrolyzed slag (HS).

peaks related to halite (NaCl), derived from the high amounts of salt used in the aluminum scrap melting process. The high background of the XRD pattern also suggest the existence of non-crystalline or amorphous phases, which may include metallic oxides such as iron oxide, among others. This presence may vary depending on the type of scrap used in the production of secondary aluminum.

Due to its high salt content, the salt slag was hydrolyzed before being used as a raw material. The main component of the hydrolyzed slag was aluminum oxide (Al_2O_3), and its content in relation to the initial composition of salt slag (Table 2) increased significantly, from 35.5% to 63.5%. This increased can be attributed to the effectiveness of the hydrolysis process, which resulted in a reduction of more than 90% in NaCl content, along with the newly formed aluminum oxides from the reaction of metallic aluminum, aluminum nitride and other aluminum compounds with water.

The chemical composition of the RHA (Table 2), shows that its main component is SiO_2 (73.5 wt.%), followed by small amounts of potassium, phosphorus, calcium, and magnesium. The XRD pattern (Fig. 4a) indicates that RHA is composed of silica in its crystalline form, cristobalite, due to the predominant presence of peak located at $2\theta = 21.8^{\circ}$ (Shinohara and Kohyama, 2004). The amorphous, crystalline or combined forms of silica are related to the ash production method and its calcination temperature. The silica contained in the ash is predominantly crystalline when high temperatures are used to calcine the rice husk (Foletto et al., 2009; Melo et al., 2014).

Due to the high LOI value (Table 2), RHA was thermally treated to eliminate the carbonaceous material. Previously, a thermal analysis was carried out to determine the optimal calcination temperature. Fig. 4b shows the TG/DTA curves. Three stages are clearly observed in TG curve. The first one, at temperature below 100 °C, corresponds to the loss of water due to humidity (2.72 wt.%). Between 200 and 600 °C, the greatest loss of mass takes place, with a value of 12.84 wt.%, which can be attributed to the combustion of carbonous material, as it is accompanied by a exothermic peak, centered around 450 °C (associated energy of 15.46 μV min mg^{-1}). Finally, a small mass loss of 1.23 wt.% can be observed between 800 and 1000 °C. This loss can be attributed to the decomposition of chlorinated compounds and/or the formation of gases containing chlorine, which occurs at high temperatures, since there is a decrease in the presence of this component, from 0.7 to <0.1 (Table 2). The total loss of mass was 16.79 % obtained by thermal analysis is quite similar to the loss of ignition (LOI) of 15.69 %. In this way, knowing the temperature required to remove the carbon content,

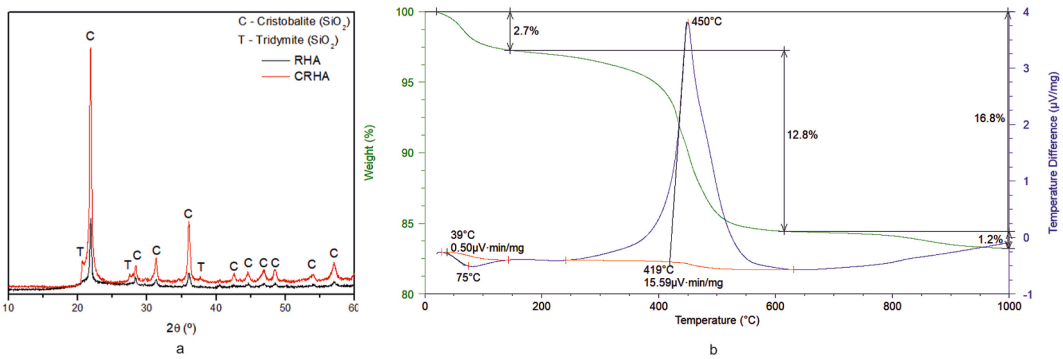

Fig. 4. (a) XRD pattern of the rice husk ash (RHA) and calcined rice husk ash (CRHA), and (b) TG/DTA curves.

the initial RHA was calcined at 800 °C for 8 h in a Thermo Concept furnace. The appearance of calcined RHA is shown in Fig. 1d and its XRD pattern (Fig. 4a) indicates that cristobalite remains the predominant component of the CRHA, but it has increased in crystallinity and other SiO_2 phase, tridymite, has developed. The LOI reduction from 15.7 to 0.2 % (Table 2) confirms the effectiveness of the calcination of the RHA.

To achieve the stoichiometric ratio of silicon for the synthesis of NaP zeolite, a silicate solution was produced from CRHA, since it is composed of high crystalline cristobalite (Fig. 4a), which is a very stable form of SiO_2, and accordingly makes it difficult to react properly (especially at lower temperatures), with aluminate ions. The silicate solution consisted mainly of Na (69.7 g L^{-1}) and Si (58.3 g L^{-1}), with minor participation of other elements (Table 3).

3.2. Statistical analysis of the waste-based zeolite synthesis

The synthesis of the waste-based zeolites was carried out using hydrolyzed slag and silicate solution from calcined rice husk ash as aluminum and silicon sources, respectively. The effect of the synthesis parameters on the zeolites crystallization was explored using a CCRD (Table 1). According to the experimental design proposed, hydrothermal temperatures between 85 and 115 °C were tested using different reaction times (2–28 h). The 2^2-CCRD data matrix with the sample names, factor values and responses is presented in Table 4.

Most of the conditions tested showed a degree of crystallization of over 70% for the waste-based NaP zeolites, with the exception of runs 1 and 7, in which lower reaction times were used. In run 3, although a low reaction time (6 h) was also used, the hydrothermal temperature was higher (110 °C), resulting in a sample with 72% crystallinity. Using a high hydrothermal temperature (110 °C) for the longest reaction time (24 h), run 4 resulted in the highest crystallinity, 73.9%. The estimated effects, presented in Table 5, were based on the p-value. At a significance level of 95%, the planning determined that, in the implemented model, the interaction ($Q_1 vs Q_2$) between the variables (time and temperature) had a significant influence ($p < 0.05$) on the crystallization of synthetic zeolites. In addition, the independent variables temperature (Q_1) in linear form, and time (Q_2) in both linear and quadratic form, were also significant ($p < 0.05$) and influenced the crystallization process. The crystallinity of the waste-based zeolites is linearly dependent on the hydrothermal temperature and reaction time, and their effects are positive (3.2941 and 4.1572, respectively), i.e., when increasing temperature and time there is also an increase in the degree of crystallization of the zeolite. Coefficient of determination (R^2) provides the measure of the proportion of variation explained by the regression equation in relation to the variation in responses. For the zeolite crystallization, an $R^2 = 0.8367$ was obtained, indicating that the model is able to explain approximately 83.7% of the

Table 3
Quantitative chemical composition of silicate solution from CRHA (ICP–OES, in g L^{-1}).

Na	Si	K	S	Al	Ca	Fe	Mg
69.7	58.3	4.1	0.27	0.14	0.007	0.006	<0.001

Table 4
Factorial design (2^2) results for waste-based zeolite synthesis using HS and CRHA.

Run n°	Factors				Sample	Responses
	Hydrothermal Temperature		Reaction Time			
	Factor Level	Temperature (°C)	Factor Level	Time (h)		Crystallinity (%)
1	−1	90	−1	6	Z90-6	63.2
2	−1	90	1	24	Z90-24	71.4
3	1	110	−1	6	Z110-6	72.0
4	1	110	1	24	Z110-24	73.9
5	−1.414	85	0	15	Z85-15	70.3
6	1.414	115	0	15	Z115-15	72.1
7	0	100	−1.414	2	Z100-2	68.5
8	0	100	1.414	28	Z100-28	72.7
9	0	100	0	15	Z_A100-15	72.0
10	0	100	0	15	Z_B100-15	71.4
11	0	100	0	15	Z_C100-15	71.5

Table 5
Estimated effects for the crystallization of the waste-based zeolites.

	Coefficient	Effect	Standard error	t(2)	p-value
Temperature (L)	Q_1	*3.2941*	*0.2205*	*14.9382*	*0.0045*
Temperature (Q)	Q_{12}	−0.6844	0.2461	−2.7808	0.1086
Time (L)	Q_2	*4.1572*	*0.2301*	*18.0673*	*0.0030*
Time (Q)	Q_{22}	*−1.6467*	*0.2797*	*−5.8873*	*0.0277*
Temperature vs Time	$Q_1 vs Q_2$	*−3.1500*	*0.3214*	*−9.7992*	*0.0103*

L: Linear; Q: Quadratic; p-value significant at $p < 0.05$.

variations in the crystallization of the obtained zeolites. The variance analysis (ANOVA) was performed, and it was found that for the crystallization of the zeolites, $F_{calculated} > F_{tabulated}$ (Table 6), confirming the statistical representativeness of the sample distribution. Therefore, the ANOVA regarding the crystallization of the obtained zeolites demonstrated the validity of the model within the 95% confidence interval, indicating no need for adjustments within the examined range. This outcome indicates an excellent reproduction of the experimental samples.

According to (Núñez-Gómez et al., 2017), the linear and quadratic coefficients, along with their interations, are part of the template employed to construct the surface that define the optimal conditions for maximizing the response. Response surface and contour curve graphics (Fig. 5) allow visualization of the optimal (or near optimal) values, in which the combination of variables led to these better responses. The results indicate that zeolite crystallization was maximum (>74%) when the synthesis was performed at high temperatures (>115 °C), even with shorter reaction times of up to 18 h (Fig. 5). In other conditions, the interaction between these two variables determines the degree of crystallization of the obtained zeolites. Using longer reaction times, high crystallinity can be obtained even at lower temperatures. At temperatures of up to 100 °C, synthesis times of over 24 h are required to obtain crystallinity of up to 74%. The same occurs at shorter times using higher hydrothermal temperatures. A synthesis conducted for 6 h can result in a zeolite with a degree of crystallinity of up to 72% when using a temperature of 110 °C.

This indicates that there was variation in the crystallization process of the synthetic zeolites related to the hydrothermal temperature and reaction time, in agreement with the corresponding p-value discussed above (Table 5). The critical values statistically determined using the STATISTICA® 13.3 software, were a hydrothermal temperature of 105 °C and a reaction time of 20 h. An experiment with these determined factor values was conducted to assess the validity of the results, as other experimental factors were not taken into account in the statistical analysis. In this sample (named Z_{oc}105-20), a high degree of crystallinity was observed (73.4%), even though an intermediate temperature and reaction time were used. This value was only slightly below than that of run 4, which resulted in a crystallinity of 73.9%. However, in this case, the synthesis was carried out at a higher temperature (110 °C) and using a longer reaction time (24 h). The observed difference in terms of crystallinity of the obtained zeolites is very small considering the energy and time savings between the two processes, so the results demonstrate the suitability of CCRD planning to determine the optimum synthesis conditions.

Equation (3) represents the model describing the degree of crystallization (%). A quadratic regression of the functional variable for the crystallinity response is proposed, where 't' represents the reaction time and 'T' denotes the hydrothermal temperature.

$$\text{Crystallinity (\%)} = 23.172 + 0.427\ T + 2.240\ t + 0.009\ t^2 - 0.0175\ t\ T \quad (3)$$

Table 6
Analysis of variance for the waste-based zeolite crystallization for the 2^2 factorial design.

Variation source	SS	df	MS	F		*p*
				Calc.	Tab.[a]	
Regression	68.0548	3	22.6849	11.153	4.347	<0.05
Sediments	14.2416	7	2.0345			
Total	82.2963	10				

SS: sum of square; df: degree of freedom; MS: mean of square; F: Fisher's ratio; p: probability.
[a] Tabulated values (Box et al., 1978).

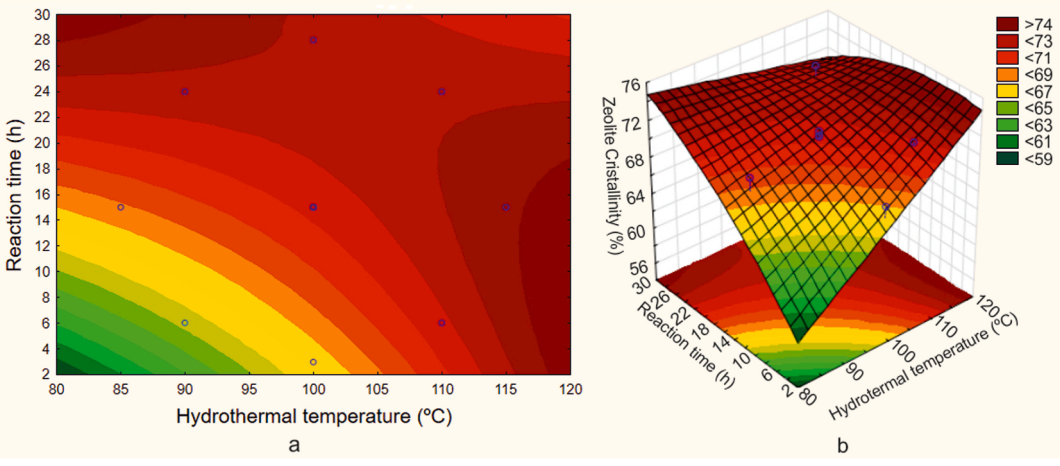

Fig. 5. (a) Response surface and (b) contour curve for waste-based zeolite crystallization.

3.3. Characterization of the synthesized waste-based zeolites

The XRD spectra of the waste-based zeolites synthesized under different conditions (Runs 1 to 11, Table 4) are shown in Fig. 6.

All samples presented a profile characteristic of tetragonal type P zeolite (NaP, $Na_6Al_6Si_{10}O_{32}{\cdot}12H_2O$). According to Hansen et al. (1993), the different symmetries (cubic, tetragonal or orthorhombic) depend on the synthesis conditions. In this regard, Sánchez-Hernández et al. (2016) also obtained a NaP zeolite with tetragonal symmetry, using different aluminum waste (sleeve filter fine dust from slag milling) and commercial waterglass by hydrothermal synthesis at 120 °C for 6 h. Padilla et al. (2022) synthesized a NaP-type zeolite with cubic symmetry from salt slag and commercial silicate at 100 °C for 24 h. This corroborates the influence of the experimental synthesis conditions, but also indicates that the starting reagents used affect the symmetry of the zeolite crystals.

The XRD pattern of the obtained zeolites exhibits narrow, well-defined peaks, with the most intense reflection centered around 28.1° (2θ), corresponding to the hkl [301]. The difference in the intensity and FWHM of this peak with the synthesis conditions can be seen in Fig. 7.

Table 7 shows the intensity, diffraction angle (2θ) and Full Width at Half Maximum (FWHM) of the most intense diffraction peak [301] for each waste-based zeolite synthesized, as well as the crystallite size (D_{hkl}) determined using the Scherrer equation (**Equation (1)**) (presented in Section 2.1). The obtained zeolites showed the most intense peak (3042–5063 counts) centered between 28.07° and 28.14° (2θ), and the crystallite sizes ranged from 21 to 28 nm. For the samples corresponding to the central points of the CCRD (Z_A100-15, Z_B100-15 and Z_C100-15), determined to assess the repeatability of the results, the average values of the peak parameters were calculated. A maximum intensity of 4490 ± 331 counts was observed, centered on the diffraction angle 28.08° ± 0.01°, with a FWHM of 0.33° ± 0.03° and a crystallite size of 25 nm ± 2 nm.

In addition to the peak parameters and crystallite sizes, the semi-quantification of the most crystalline phases for the Z90-24, Z110-6, Z110-24 and Z_{OC}105-20 waste-based zeolites (obtained using the Diffrac.Suite EVA software) and the yield of the synthesis reaction are shown in Table 8.

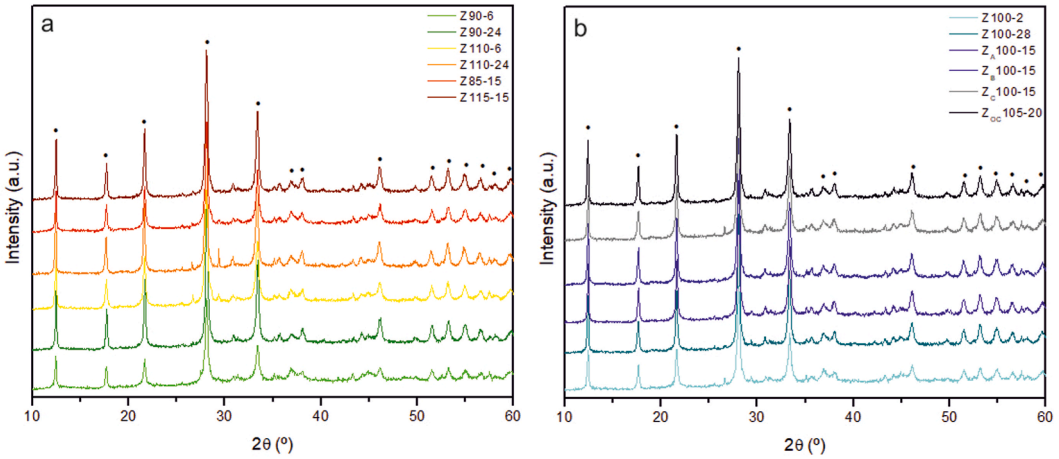

Fig. 6. XRD spectra of zeolite materials synthesized under various parameter settings: (a) Run 1-Run 6 and (b) Run 7-Run 11 and Z_{OC}105-20 (• = NaP zeolite, reference file ICDD PDF = 39–0219).

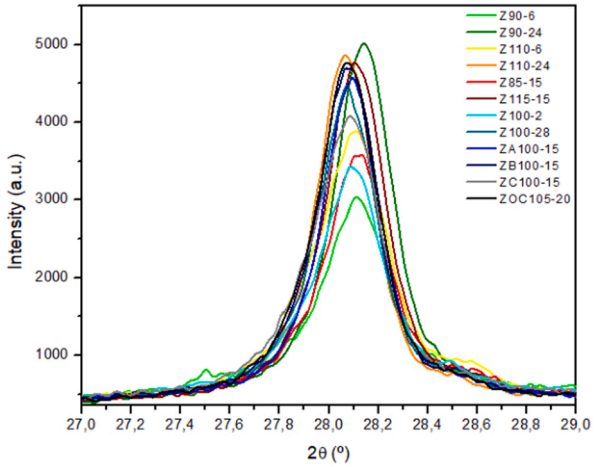

Fig. 7. Most intense reflection of the synthesized waste-based zeolites.

Table 7
Peak parameters (intensity, 2θ and FWHM) and crystallite sizes (D_{hkl}) of the synthesized waste-based zeolites.

Sample	Intensity (counts)	2θ (°)	FWHM (°)	D_{hkl} (nm)
Z90-6	3042	28.11	0.3950	21
Z90-24	5063	28.14	0.3117	26
Z110-6	3910	28.09	0.3901	21
Z110-24	4892	28.07	0.2968	28
Z85-15	3270	28.11	0.3513	23
Z115-15	4821	28.11	0.3183	26
Z100-2	3456	28.09	0.3706	22
Z100-28	4509	28.07	0.3165	26
Z_A100-15	4619	28.09	0.3064	27
Z_B100-15	4738	28.07	0.3158	26
Z_C100-15	4114	28.07	0.3614	23
Z_{OC}105-20	4778	28.07	0.3280	25

Table 8
Semi-quantification of the NaP zeolite (reference file ICDD PDF = 39–0219) and yield of the synthesis reaction.

Sample	NaP (%)	Yield (Kg zeolite/Kg HS)
Z90-24	89.1	1.70
Z110-6	82.6	1.69
Z110-24	83.6	1.75
ZOC105-20	90.8	1.77

The semi-quantitative analysis of the samples shows that the waste-based zeolite synthesis resulted in the formation of materials with high NaP zeolite content, ranging from 82.6% (Z110-6) to 90.8% (Z_{OC}105-20). No other type of zeolite was observed. However, small amounts of compounds from salt slag that did not react completely could be tentatively identified in these samples, including corundum and spinel. Furthermore, for each kg of hydrolyzed slag used in the synthesis process, between 1.69 and 1.77 kg of zeolites can be produced. The zeolite synthesized at 110 °C for 24 h (Z110-24) showed a slightly higher yield (1.75) and percentage of NaP zeolite (83.6%) compared to the synthesis carried out for 6 h (Z110-6), which were 1.69 and 82.6%, respectively. Also, the longer reaction time increased the crystallinity of this sample (73.9%) compared to the previous one (72.0%) (Table 4). Despite the lower yield (1.70) and crystallinity (71.4%) compared to Z110-24, sample Z90-24 has significantly higher amount of NaP zeolite, 89.1% compared to 83.6%. Comparing samples Z90-24 and Z110-6, it can be observed that a longer reaction time has a greater impact than temperature on crystallinity, resulting in a higher content of NaP zeolite in the synthesized material. Although the Z_{OC}105-20 sample presents a slightly lower degree of crystallinity (73.4%) than that obtained for Z110-24 (73.9%), it was the one that obtained the highest yield (1.77) and the highest content of NaP zeolite (90.8%). This confirms that the optimal experimental conditions for hydrothermal synthesis, obtained through CCRD, are a moderate temperature of 105 °C and a reaction time of 20 h.

The textural properties of the selected zeolites Z90-24, Z110-6, Z110-24 and Z_{OC}105-20, including specific surface area (S_{BET}), external surface area (S_{Ext}) and pore size, determined from adsorption isotherms/N_2 desorption (Fig. 8a), as well as their cation exchange capacity (CEC) are presented in Table 9.

The nitrogen adsorption/desorption isotherms of the zeolites showed the same type IV behavior typical of mesoporous materials (2–50 nm). The mesoporous characteristic of NaP zeolite possibly results from the assembly of nanometric crystallites that form its

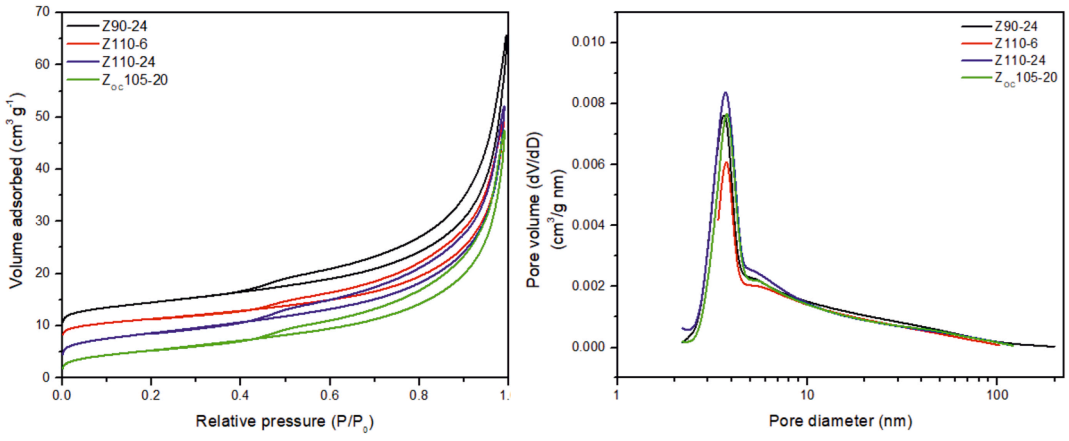

Fig. 8. (a) Nitrogen adsorption/desorption isotherms and (b) distribution of pore diameter of the waste-based NaP zeolites.

Table 9
Textural properties and CEC of the synthesized waste-based zeolites.

	S_{BET} ($m^2\ g^{-1}$)	S_{Ext} ($m^2\ g^{-1}$)	Micropore volume ($x10^{-4}\ cm^3\ g^{-1}$)	Pore size (nm)	CEC (meq g^{-1})
Z90–24	22.45	22.11	1.86	3.80	3.55 ± 0.002
Z110–6	18.49	17.53	4.82	3.79	2.86 ± 0.054
Z110–24	23.18	23.57	Not determined	3.80	3.23 ± 0.035
Z_{OC}105–20	21.11	20.77	1.89	3.80	3.67 ± 0.039

aggregates (Sayehi et al., 2020). In all cases, the hysteresis loop (H3 type – according to the IUPAC classification) was observed at P/P_0 range between 0.45 and 0.98 (maximum pressure) indicating the presence of many nanometer-sized pores and characterizing solid materials with slit-shaped pores of non-uniform sizes or shapes (Bandura et al., 2015). The pore size distribution curve, acquired by the BJH method (Fig. 8b) shows a mesoporous distribution with a predominant pore size of 3.8 nm observed in all samples. The smaller peaks located at 5.4 nm (Z90-24, Z110-6 and Z110-24) and 5.6 nm (Z_{OC}105-20) could indicate a secondary pore size.

In terms of S_{BET} (Table 9), values between 18.49 and 23.18 $m^2\ g^{-1}$ were obtained. The observation of tabulated values suggests that the difference in surface area of the obtained zeolites was influenced to a greater extent by the reaction time than by the synthesis temperature. The Z_{OC}105-20 zeolite, synthesized under optimal experimental conditions, showed a S_{BET} of 21.11 $m^2\ g^{-1}$ and S_{ext} = 20.77 $m^2\ g^{-1}$. This small difference indicates the low micropore volume (1.89 × 10^{-4} $cm^3\ g^{-1}$) of the zeolite. The small micropore volume observed in the samples is probably due to the shape (bottleneck) of the micropores, which interferes with the entry of the gas and, consequently, its determination (Sharma et al., 2016). S_{BET} values were higher when compared to those obtained for NaP-type zeolites using other aluminum waste (14.2 $m^2\ g^{-1}$) (Sánchez-Hernández et al., 2016), salt slag (17.0 $m^2\ g^{-1}$) (Padilla et al., 2022) and fly ash (18.5 $m^2\ g^{-1}$) (Liu et al., 2018). Although differences in the degasification conditions may affect these values of S_{BET}, the results obtained in this work indicate that the waste-based NaP zeolite owing potential characteristic to be used as an adsorbent material.

The CEC values for NH_4Cl ranged from 2.86 to 3.67 meq g^{-1} for the synthesized NaP zeolites. The highest CEC (3.67 meq g^{-1}) was obtained for the zeolite Z_{OC}105-20. This value is higher than those reported for waste-based NaP-type zeolites. Using aluminum waste, as already mentioned, Padilla et al. (2022) and Sánchez-Hernández et al. (2016), obtained a CEC of 2.12 and 2.73 meq g^{-1}, respectively. From coal fly ash, Cardoso et al. (2015) obtained CEC of 2.6 meq g^{-1} through hydrothermal synthesis with 3 M NaOH at 100 °C for 24 h. Musyoka et al. (2012) achieved a CEC of 2.98 meq g^{-1} in a two-step synthesis at 100 °C for 48 h. Additionally, Zhou et al. (2023) reported a CEC of 2.58 meq g^{-1} for zeolite synthesized in a two-step process with a microwave reaction at 180 °C for 2 h after 12 h of stirring. This characteristic also enables zeolite to be used as an adsorbent.

The morphology of the Z90-24, Z110-6, and Z110-24 zeolites at different magnifications is shown in Fig. 9. All the samples exhibited a homogeneous 'cauliflower-like' morphology, characteristic of NaP-type structures (Sánchez-Hernández et al., 2016). In the figure, it can be observed that the units constituting the aggregates are particles measuring between 420 and 990 nm, while the joining of these units forms conglomerates measuring between 2 and 5 μm.

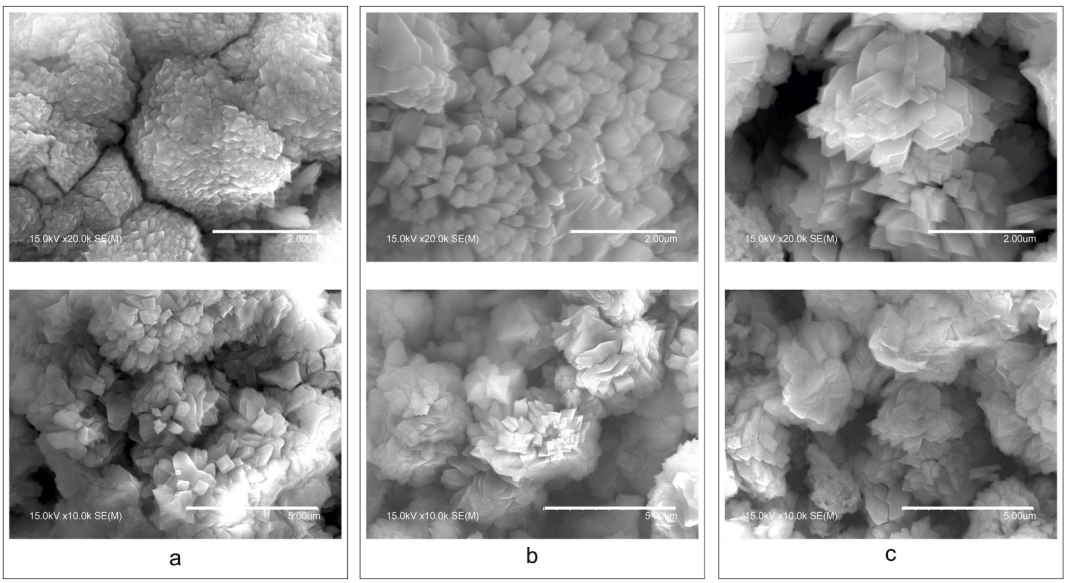

Fig. 9. SEM images of the waste-based zeolites (a) Z90-24, (b) Z110-6 and (c) Z110-24, at different magnifications.

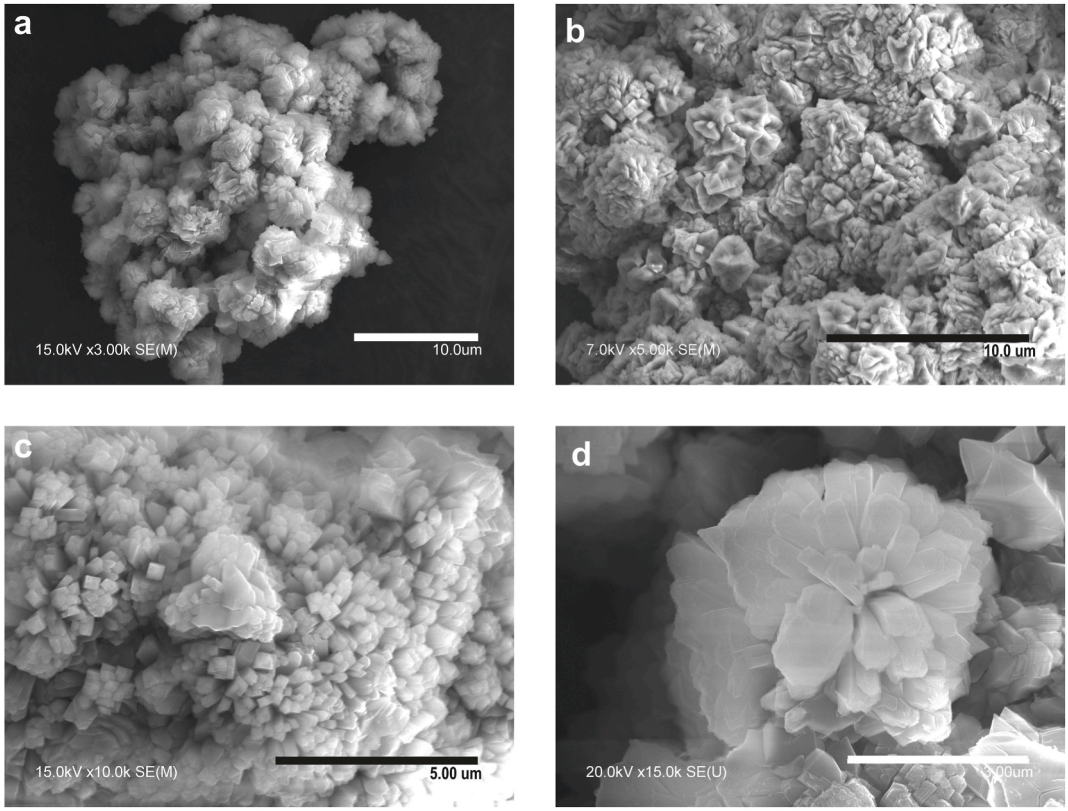

Fig. 10. SEM images of the waste-based zeolite synthesized under the optimal conditions at different magnifications.

Fig. 10 shows the SEM images at different magnifications of the Z_{OC}105-20 zeolite. This NaP zeolite exhibited a morphology composed by agglomerates of around 10–50 μm (Fig. 10a and **b**). As can be seen at high magnification (Fig. 10c and **d**), these clusters were formed by smaller secondary aggregates with defined contours growing in different directions.

4. Conclusion

In this study, hazardous salt slag (aluminum source) and rice husk ash (silicon source) were valorized through their use as uncommon raw materials for the production of zeolites with excellent sorbent characteristics and promising applications. Almost all the tested synthesis conditions showed a degree of crystallization greater than 70% for the waste-based NaP zeolites. It was found that the variables of time and temperature, separately and the interaction between them, exerted a significant influence on the crystallization of the zeolites. The optimal experimental conditions (105 °C and 20 h), statistically determined, resulted in a zeolite with a high degree of crystallinity (73.4%) and containing more than 90% zeolitic material. ANOVA analysis regarding the crystallization of the obtained zeolites indicated that the valitiy of the model within the 95% confidence interval, and no adjustment were required within the evaluated range. This led to an outstanding reproducibility of experimental samples. Both S_{BET} (21.11 $m^2\ g^{-1}$) and CEC (3.67 meq g^{-1}) showed higher values than those reported by other authors for the synthesis of NaP-type zeolites using different wastes, suggesting adequate properties of the waste-based NaP-zeolite for effluent treatments via adsorption and ion exchange mechanisms. The co-recycling of both hazardous aluminum and agri-food wastes into zeolites promotes an industrial symbiosis and can be considered a sustainable alternative in waste management, generating value-added materials and greatly contributing to environmental preservation.

CRediT authorship contribution statement

Magali Teresinha Ritter: Writing – original draft, Investigation, Formal analysis, Data curation. **María Ángeles Lobo-Recio:** Writing – review & editing. **Isabel Padilla:** Writing – review & editing, Supervision, Methodology. **Maximina Romero:** Writing – review & editing. **Aurora López-Delgado:** Writing – review & editing, Supervision, Conceptualization.

Declaration of competing interest

The authors declare that they have no known competing financial interests or personal relationships that could have appeared to influence the work reported in this paper.

Data availability

No data was used for the research described in the article.

Acknowledgements

This research was financed by the LIFE Project 101114027 — LIFE22-ENV-ES-Z-ONA4LIFE, and Eduardo Torroja Institute for Construction Sciences (IETcc-CSIC), Spain. This work was supported by the Brazilian National Council of Scientific and Technologic Development (CNPq), Brazil and Coordination for the Improvement of the Higher-Level Personnel (CAPES), Brazil-finance code 001. The authors thank Herba Ricemills S.L.U (Spain) for providing the rice husk ash sample and Alusigma S.A (Spain) for supplying the salt slag sample.

References

Abdel-Hameed, R., Farghaly, E.E., Abdel-Aal, E.A., Ibrahim, I.A., Ahmed, M.A., Abdel-Messih, M.F., Abdel Khalek, M.A., 2020. Exploitation of industrial solid wastes for preparing zeolite as a value-added product and its kinetics as adsorbent for heavy metal ions. Physicochem. Probl. Miner. Process. 57 (1), 87–99. https://doi.org/10.37190/ppmp/128744.

Alaba, P.A., Sani, Y.M., Mohammed, I.Y., Abakr, Y.A., Daud, W.M.A.W., 2017. Synthesis of hierarchical nanoporous HY zeolites from activated kaolin, a central composite design optimization study. Adv. Powder Technol. 28 (5), 1399–1410. https://doi.org/10.1016/j.apt.2017.03.008.

Bandura, L., Franus, M., Józefaciuk, G., Franus, W., 2015. Synthetic zeolites from fly ash as effective mineral sorbents for land-based petroleum spills cleanup. Fuel 147, 100–107. https://doi.org/10.1016/j.fuel.2015.01.067.

Box, G.E.P., Hunter, W.G., Hunter, J.S., 1978. Fractional factorial design at two levels, Statistics for Experimenters: an Introduction to Design, Data Analysis, and Model Building. John Wiley & Sons, Inc, New Jersey, pp. 374–418.

Cardoso, A.M., Horn, M.B., Ferret, L.S., Azevedo, C.M.N., 2015. Integrated synthesis of zeolites 4A and Na–P1 using coal fly ash for application in the formulation of detergents and swine wastewater treatment. J. Hazard Mater. 287, 69–77. https://doi.org/10.1016/j.jhazmat.2015.01.042.

Collins, F., Rozhkovskaya, A., Outram, J.G., Millar, G.J., 2020. A critical review of waste resources, synthesis, and applications for Zeolite LTA. Microporous Mesoporous Mater. 291, 109667. https://doi.org/10.1016/j.micromeso.2019.109667.

EWC, 2001. European Waste Catalogue and Hazardous Waste List, Published by Environmental Protection Agency. Ireland. https://ec.europa.eu/eurostat/documents/342366/351806/Guidance-on-EWCStat-categories-2010.pdf/0e7cd3fc-c05c-47a7-818f-1c2421e55604 (Accessed 10 February 2024).

FAO, 2022. Food Agricult. Organizat. United Nat. 2022. Avaiable online: https://www.fao.org/home/en. (Accessed 24 January 2024).

Foletto, E.L., Castoldi, M.M., Oliveira, L.H., Hoffmann, R., Jahn, S.L., 2009. Conversion of rice husk ash into zeolitic materials. Lat. Am. Appl. Res. 39, 75–78.

Hansen, S., Hakansson, U., Landa-Canovas, A.R., Falth, L., 1993. On the crystal chemistry of NaP zeolites. Zeolites 13 (4), 276–280.

Kafshgari, L.A., Ghorbani, M., Azizi, A., Agarwal, S., Gupta, V.K., 2017. Modeling and optimization of Direct Red 16 adsorption from aqueous solutions using nanocomposite of $MnFe_2O_4$/MWCNTs: RSM-CCRD model. J. Mol. Liq. 233, 370–377. https://doi.org/10.1016/j.molliq.2017.03.047.

Liu, Y., Yan, C., Zhao, J., Zhang, Z., Wang, H., Zhou, S., Wu, L., 2018. Synthesis of zeolite P1 from fly ash under solvent-free conditions for ammonium removal from water. J. Clean. Prod. 202, 11–22. https://doi.org/10.1016/j.jclepro.2018.08.128.

Mallapur, V.P., Oubagaranadin, J.U.K., 2017. A brief review on the synthesis of zeolites from hazardous wastes. Trans. Indian Ceram. Soc. 76 (1), 1–13. https://doi.org/10.1080/0371750X.2016.1231086.

Markets and Markets. Zeolites Market by Type (Natural, Synthetic), Function (Ion-Exchange, Catalyst, Molecular Sieve), Synthetic Zeolite Application (Detergents, Adsorbent, Catalysts), Natural Zeolite Application, and Region – Global Forecast to 2026. Avaiable online: https://www.marketsandmarkets.com/Market-Reports/zeolites-market-76442083.html. Accessed on: 5 October. 2023.

Melo, C.R., Francisco, A.C., Kuhnen, N.C., Rocha, M.R., Melo, A.R., Riella, H.G., Angioletto, E., 2014. Production of zeolite from rice husk ash. Mater. Sci. Forum 798–799, 617–621. https://doi.org/10.4028/www.scientific.net/MSF.798-799.617.

Mohamed, R.M., Mkhalid, I.A., Barakat, M.A., 2015. Rice husk ash as a renewable source for the production of zeolite NaY and its characterization. Arab. J. Chem. 8 (1), 48–53. https://doi.org/10.1016/j.arabjc.2012.12.013.

Musyoka, N.M., Petrik, L.F., Gitari, W.M., Balfour, G., Hums, E., 2012. Optimization of hydrothermal synthesis of pure phase zeolite Na-P1 from South African coal fly ashes. J. Environ. Sci. Health, Part A 47 (3), 337–350. https://doi.org/10.1080/10934529.2012.645779.

NC 626, 2008. Natural Zeolites - Determination of Exchange Capacity Total Cationic - Ammonium Chloride Method.

Núñez-Gómez, D., Lapolli, F.R., Nagel-Hassemer, M.E., Lobo-Recio, M.Á., 2017. Optimization of acid mine drainage remediation with central composite rotatable design model. Energy Proc. 136, 233–238. https://doi.org/10.1016/j.egypro.2017.10.248.

Padilla, I., Romero, M., López-Andrés, S., López-Delgado, A., 2022. Sustainable management of salt slag. Sustainability 14 (9), 4887. https://doi.org/10.3390/su14094887.

Sánchez-Hernández, R., López-Delgado, A., Padilla, I., Galindo, R., López-Andrés, S., 2016. One-step synthesis of NaP1, SOD and ANA from a hazardous aluminum solid waste. Microporous Mesoporous Mater. 226, 267–277. https://doi.org/10.1016/j.micromeso.2016.01.037.

Sayehi, M., Garbarino, G., Delahay, G., Busca, G., Tounsi, H., 2020. Synthesis of high value-added Na–P1 and Na-FAU zeolites using waste glass from fluorescent tubes and aluminum scraps. Mater. Chem. Phys. 248, 122903. https://doi.org/10.1016/j.matchemphys.2020.122903.

Scherrer, P., 1918. Estimation of the size and internal structure of colloidal particles by means of röntgen, Nachrichten von der Gesellschaft der Wissenschaften zu Göttingen. 2, 96–100.

Sharma, P., Song, J.S., Han, M.H., Cho, C.H., 2016. GIS-NaP1 zeolite microspheres as potential water adsorption material: influence of initial silica concentration on adsorptive and physical/topological properties. Sci. Rep. 6 (1), 22734. https://doi.org/10.1038/srep22734.

Shinohara, Y., Kohyama, N., 2004. Quantitative analysis of tridymite and cristobalite crystallized in rice husk ash by heating. Ind. Health 42 (2), 277–285.

Shu, R., Qiao, Q., Guo, F., Dong, K., Liu, S., Xu, L., Bai, Y., Zhou, N., 2023. Controlled design of Na–P1 zeolite/porous carbon composites from coal gasification fine slag for high-performance adsorbent. Environ. Res. 217, 114912. https://doi.org/10.1016/j.envres.2022.114912.

Srivastava, A., Meshram, A., 2023. On trending technologies of aluminium dross recycling: a review. Process Saf. Environ. Protect. 171, 38–54. https://doi.org/10.1016/j.psep.2023.01.010.

Statista, 2023. Market volume of secondary aluminum worldwide in 2020, with a forecast for 2027. Avaiable online: https://www.statista.com/statistics/1306589/global-market-volume-of-secondary-aluminum. (Accessed 5 September 2023).

Tan, W.-C., Yap, S.-Y., Matsumoto, A., Othman, R., Yeoh, F.-Y., 2011. Synthesis and characterization of zeolites NaA and NaY from rice husk ash. Adsorption 17 (5), 863–868. https://doi.org/10.1007/s10450-011-9350-6.

Tran-Nguyen, P.L., Lyb, K.-P., Thanhb, L.H.V., Angkawijayac, A.E., Santosod, S.P., Trane, N.-P.-D., Tsaie, M.-L., Juc, Y.-H., 2021. Facile synthesis of zeolite NaX using rice husk ash without pretreatment. J. Taiwan Inst. Chem. Eng. 123, 338–345. https://doi.org/10.1016/j.jtice.2021.05.009.

Tsakiridis, P.E., 2012. Aluminium salt slag characterization and utilization – a review. J. Hazard Mater. 217–218, 1–10. https://doi.org/10.1016/j.jhazmat.2012.03.052.

Vasconcelos, A.A., Len, T., Oliveira, A.N., da Costa, A.A.F., Souza, A.R.S., da Costa, C.E.F., Luque, R., Filho, G.N.R., Noronha, R.C.R., do Nascimento, L.A.S., 2023. Zeolites: a theoretical and practical approach with uses in (Bio)Chemical processes. Appl. Sci. 13 (3), 1897. https://doi.org/10.3390/app13031897.

Xu, R., Pang, W., Yu, J., Huo, Q., Chen, J., 2007. Chemistry of Zeolites and Related Porous Materials: Synthesis and Structure [s.l.]. John Wiley & Sons.

Yi, S., Su, Y., Qi, B., Su, Z., Wan, Y., 2010. Application of response surface methodology and central composite rotatable design in optimizing the preparation conditions of vinyltriethoxysilane modified silicalite/polydimethylsiloxane hybrid pervaporation membranes. Sep. Purif. Technol. 71 (2), 252–262. https://doi.org/10.1016/

j.seppur.2009.12.005.
Zhou, Q., Jiang, X., Qiu, Q., Zhao, Y., Long, L., 2023. Synthesis of high-quality Na P1 zeolite from municipal solid waste incineration fly ash by microwave-assisted hydrothermal method and its adsorption capacity. Sci. Total Environ. 855, 158741. https://doi.org/10.1016/j.scitotenv.2022.158741.